AGU PUBLICATIONS

Geophysical Research Letters

RESEARCH LETTER
10.1002/2017GL076235

Key Points:
- Lyman-α signatures of proton aurora have been observed with SPICAM on board Mars Express
- Six limb profiles show unambiguous intensity enhancements between 120 and 150 km
- All detections are related to the arrival of a coronal mass ejection or a corotating interaction region at Mars

Correspondence to:
B. Ritter,
b.ritter@uliege.be

Citation:
Ritter, B., Gérard, J.-C., Hubert, B., Rodriguez, L., & Montmessin, F. (2018). Observations of the proton aurora on Mars with SPICAM on board Mars Express. *Geophysical Research Letters*, *45*. https://doi.org/10.1002/2017GL076235

Received 31 OCT 2017
Accepted 21 DEC 2017
Accepted article online 29 DEC 2017

Observations of the Proton Aurora on Mars With SPICAM on Board Mars Express

B. Ritter[1,2], J.-C. Gérard[1], B. Hubert[1], L. Rodriguez[2], and F. Montmessin[3]

[1]LPAP, Université de Liège, Liège, Belgium, [2]Royal Observatory of Belgium, Brussels, Belgium, [3]LATMOS-CNRS/IPSL/Université de Versailles-St Quentin-en-Yvelines, Guyancourt, France

Abstract We report observations of the proton aurora at Mars, obtained with the Spectroscopy for the Investigation of the Characteristics of the Atmosphere of Mars (SPICAM) ultraviolet spectrograph on board Mars Express between 2004 and 2011. This is a third type of UV aurora that is discovered on Mars, in addition to the discrete and diffuse nightside aurora. It is observed only on the dayside as it is produced by the direct interaction of solar wind protons with the upper atmosphere. The auroral signature is an enhancement of the Lyman-α emission in the order of a few kilorayleighs. The proton aurora features peak emissions around 120 to 150 km. From the full SPICAM database, limb observations have been investigated and six clear cases have been found. We identify either coronal mass ejections and/or corotating interaction regions as triggers for each of these events.

1. Introduction

On Mars, different types of aurora have been detected through their emissions in the ultraviolet. The *discrete aurora* was first reported by Bertaux et al. (2005), who observed spatially confined auroral features in a limb scan of the Spectroscopy for the Investigation of the Characteristics of the Atmosphere of Mars (SPICAM) UV spectrometer (Bertaux et al., 2006) on board Mars Express (MEX). Subsequently, limb and nadir observations of the discrete aurora were reported, revealing that these aurorae are linked to the topology of the crustal magnetic field of Mars (Gérard et al., 2015; Soret et al., 2016). The *diffuse aurora* was observed by the Imaging Ultraviolet Spectrograph (IUVS) on board the Mars Atmosphere and Volatile Evolution (MAVEN) spacecraft and reported by Schneider et al. (2015). This auroral type is neither restricted in location nor linked to the Martian magnetic field. Instead, it is thought to be globally extended and is closely correlated to solar wind activity. Both, discrete and diffuse aurora, are observed on the Martian nightside.

Here we report SPICAM observations of a third type of aurora observed on the dayside in the ultraviolet, the *proton aurora*. It was first found in observations made with IUVS on board MAVEN and was reported by Deighan and colleagues at the AGU Fall Meeting in 2016. The proton aurora is produced by solar wind protons precipitating in the atmosphere. It has long been known at Earth (e.g., Eather, 1967) where it was discovered through the hydrogen Balmer lines in the visible (Vegard, 1939). It also manifests in the ultraviolet as Lyman-α emission of excited hydrogen at 121.6 nm and has been mapped in the terrestrial aurora (Gérard et al., 2001; Hubert et al., 2001).

Mars has a hydrogen corona that extends up to several thousands of kilometers (Chaufray et al., 2008). Solar wind protons interact with the corona through charge exchange and produce thereby a beam of neutral hydrogen at solar wind speeds (e.g., Barabash et al., 1995; Kallio et al., 1997). The production rate of these energetic neutral atoms (ENAs) depends on the solar wind flux and has been recently measured and characterized (Halekas et al., 2015, 2017; Wang et al., 2013). A mixture of hydrogen ENAs and solar wind protons penetrates deep into the Martian atmosphere (Futaana et al., 2006; Lundin et al., 2004). As the density increases, the particles interact with atmospheric particles by (in)elastic collisions, momentum and energy transfer, ionization, charge transfer, and electron capture with the main constituents (M) of the atmosphere ($M = CO_2$, CO, and O). The corresponding collisional processes can be described by (e.g., Gérard et al., 2001; Shematovich et al., 2011)

$$H_f^+(H_f) + M \quad \rightarrow \quad \begin{cases} H_{f'}^+\left(H_{f'}\right) + M^* \\ H_{f'}^+\left(H_{f'}\right) + M^+ + e^- \\ H_{f'}\left(H_{f'}^+\right) + M^+(M) + (e^-) \end{cases} \tag{1}$$

where Lyman-α emission is produced by spontaneous decay of the resulting fast (excited) hydrogen atoms (H_f) from the upper (2p) state to the ground state (1s). Most of the auroral Lyman-α line profile is optically thin and much wider compared to the optically thick emission by thermal hydrogen atoms. Hence, it can be observed as an enhancement in the integrated Lyman-α emission.

The auroral signature we look for in this work is an addition in intensity to the always present Lyman-α resonance scattering airglow limb profile at altitudes between 120 and 150 km resulting from the collisional processes described before. The enhancement at Mars was modeled for solar wind protons up to 1 keV by Kallio and Barabash (2001), who predicted a possible maximum intensity in excess of 100 R in Lyman-α between 120 and 130 km. At these altitudes, for nominal solar wind conditions, the Lyman-α airglow would hardly allow detection of this additional contribution. Leblanc et al. (2002) concluded that for solar energetic particles more Lyman-α photons are produced and expected excess intensities of 0.2 to 1 kR. Therefore, in the case of increased solar flux density or energetic solar particle occurrence, the enhancement is likely to be observed as a proton aurora. The main driver of such events could be coronal mass ejections (CMEs) and corotating interaction regions (CIRs), as both can create regions of enhanced solar wind density that can reach the Martian environment and create/affect the aurora.

CMEs are large dynamical events in which solar plasma is ejected into interplanetary space (for a review see Webb & Howard, 2012). Furthermore, fast CMEs can drive a fast forward shock in front of them (Kilpua et al., 2015, and references therein), creating a region of dense plasma between the shock and the CME (sheath). Peaks in density have also been detected in the trailing part of CMEs (Rodriguez et al., 2016). CMEs are also associated with elevated magnetic fields. Through the solar rotation, fast solar wind coming from coronal holes and slow wind from coronal streamers interact. The fast wind compresses and deflects the slower and denser slow wind ahead of it. A CIR is the thereby created region of interaction, which rotates along with the Sun. Due to compression, they can create regions of enhanced plasma density, temperature, and magnetic field (for more details see Jian et al., 2006).

In this study, we examine the full SPICAM database in order to obtain Lyman-α limb profiles in which this signature could be present and correlate our findings with possible triggering from solar events.

2. Instrument Description

The observations used in this study were performed with the SPICAM UV spectrometer on board the MEX spacecraft. MEX was inserted into a quasi-polar orbit of 6.7 h with the pericenter near 300 km and the apocenter at 10,100 km. SPICAM was designed to observe in limb and in nadir mode and could also perform stellar and solar occultation measurements. The ultraviolet spectrometer covers a spectral range from 118 to 310 nm. The entrance slit is divided in two parts, the narrow part having a field of view of 0.02° × 1.9° with a spectral resolution of ~1.5 nm and the wide part with a field of view of 0.2° × 0.98° enabling observations of weaker sources at the expense of spectral resolution (~6 nm). Along this slit, five spatial bins record photon fluxes, two in the narrow part of the slit (bins 1 and 2), two in the wide part of the slit (bins 4 and 5), and one measures fluxes in both parts (bin 3). Data from bin 3 are not used in this study. Each of the five bins provides one spectrum per second, but the flux integration time for each spectrum is 640 ms, and additional 340 ms is allocated to digital onboard data processing. Each spectrum is the sum of N individual CCD line spectra, with N = 2, 4, 8, 16, or 32. The observations reported here were collected with binning parameters of 16 and 32. During each orbit, one or more observation sequences are recorded. Regardless if a second or more sequences were recorded in the same orbit, the naming of the observations used here is "orbit number/sequence". One sequence typically lasts 20 to 30 min, and during each sequence more than 1,000 individual spectra are obtained, in which one spectrum corresponds to a 1 s time frame.

During limb observations, the spacecraft is kept in a fixed inertial attitude and records the integrated emission along the line of sight (LOS) as it skims the limb tangentially. As the spacecraft passes at pericenter, the tangent point (TP, the point of the LOS that is closest to the Martian surface) will first decrease in altitude (ingress scan) down to a minimum altitude and then increase (egress scan). A detailed description of SPICAM, the calibration, and the observing modes can be found in Bertaux et al. (2006) and Leblanc et al. (2006).

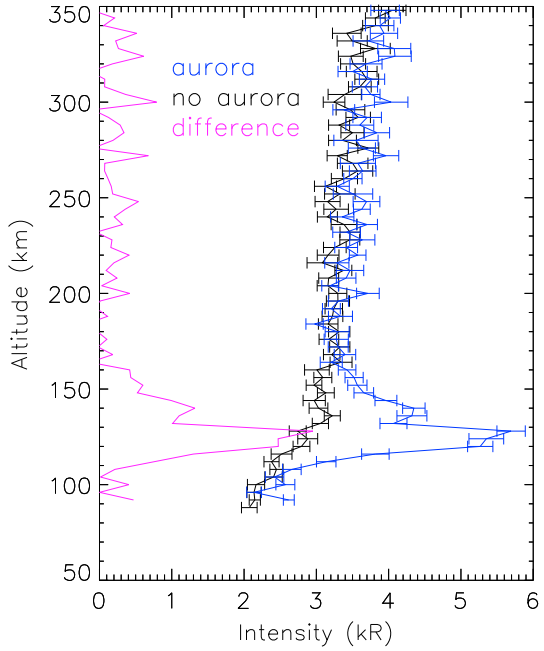

Figure 1. Lyman-α intensity profile plotted versus the tangent point altitude for an auroral (blue, Orbit 1426/1 egress) and a nonauroral case (black, Orbit 1414/2 egress). Parameters of both orbits are listed in Table 1. The difference between the two profiles is shown in magenta.

3. Data Selection and Processing

3.1. SPICAM Data

Level 1A data are used from the SPICAM database and cleaned from saturated pixels, cosmic ray effects, electronic noise, dark current, and erroneous data. Calibration was performed with the latest gain and "efficient area" curves (Montmessin et al., 2017), and analog to digital unit values were converted into photon fluxes. Observations with nonappropriate high-voltage settings in the instrument were discarded. We selected only limb observations of the Martian dayside that contain measurements during which the tangent point was between 110 and 200 km above the Martian limb. A linear background between 119 and 124 nm was subtracted in order to obtain the true Lyman-α intensity. Observations that were affected by stray light or in which the background subtraction fit was unreliable due to a too large background signal were discarded. Initially, all data processing was done separately for wide and narrow bins, while the data from the two wide bins and the data from the two narrow bins, respectively, were merged for better statistics. A total of 143 orbit sequences was selected. Of these, 54 observations provided data in the narrow bins only, 72 in the wide bins only and for 17 observations, both narrow and wide bins provided simultaneous measurements. For these observations wide and narrow bin data were merged.

Spectra have been integrated between 119 and 124 nm for each second of the respective observation sequence. As the time sequence corresponds to a range of altitudes, the integrated Lyman-α intensities were binned in 4 km intervals and the mean values of each interval plotted versus altitude (Figures 1 and 2a–2f). The horizontal bars indicate the 1 sigma standard error on the mean in each bin. Ingress and egress observations are plotted separately.

3.2. Search for Auroral Signatures

We expect to observe an increase in the Lyman-α intensity as a function of altitude, with an emission peak in the altitude range of 120 to 150 km. The altitude profiles were inspected visually and a clear case of a proton auroral signature was identified in MEX Orbit 1426/1. Figure 1 shows the egress altitude profile of this scan (blue). Overlaid is the egress profile from Orbit 1414/2 (black), which does not feature an auroral signature. This profile has been recorded less than 4 days before the aurora, which is the closest observation in time in the data set. The observational parameters are very similar for both orbits (Table 1), which justifies subtracting one from the other. The difference of these profiles is plotted in magenta, clearly showing the enhancement of the Lyman-α emission of about 3 kR between 110 and 150 km.

In parallel, an automatic approach was applied. The emission integrated between 120 and 150 km was calculated and compared to the intensity integrated between 160 and 190 km. Whereas the distribution of this ratio $R_{int} = I_{[120:150]km}/I_{[160:190]km}$ spreads from 0.7 to 1.4 for all selected observations, most of them have a ratio below unity (e.g., Orbit 1414/2 shown in Figure 1 has $R_{int} = 0.89$). Following this distribution, observations with a significant increase compared to the emission at higher altitudes (≥10%) were considered auroral candidates.

3.3. Search for Solar Events Triggering the Proton Aurora

After identification of the auroral candidates, we examined solar and interplanetary data in order to link CMEs and/or CIRs to the times when a proton aurora was observed at Mars. Therefore, we used remote sensing and in situ data from spacecraft located at the Sun-Earth L1 point or on Earth orbit (SOHO, ACE, and GOES).

In order to check for CMEs, we searched the SOHO LASCO CME catalogue for events happening 4 to 7 days before the date of the aurora (the time window was selected in order to account for CME travel times to Mars considering typical CME velocities) and directed toward the location of Mars. For the events after 2007, we also checked the HELCATS ARRCAT catalogue (Möstl et al., 2017), which contains predicted arrivals of

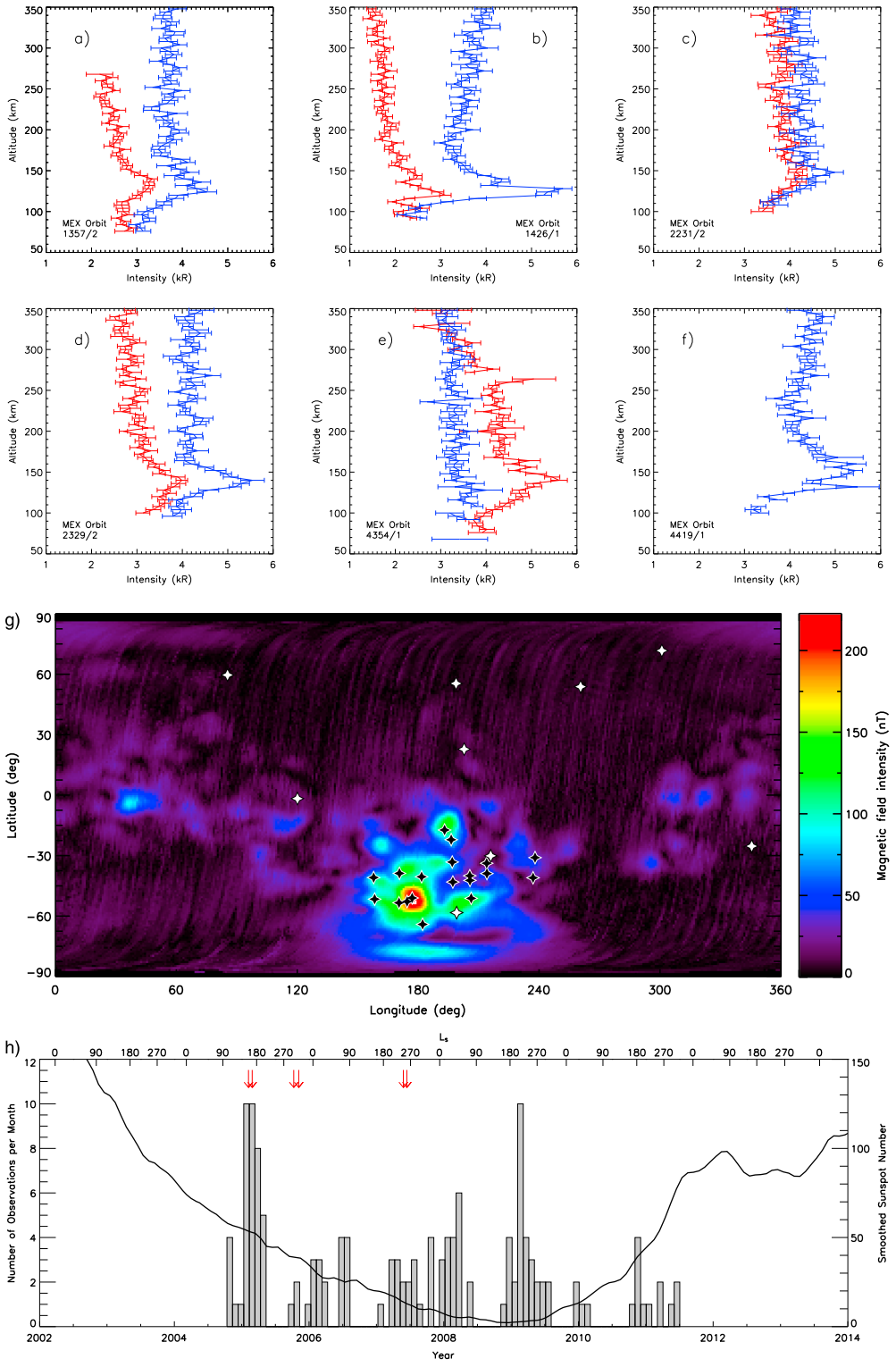

Figure 2. (a–f) The Lyman-α limb profiles of the six orbits during which aurorae have been observed are shown (Table 1, in total nine auroral limb profiles). Ingress observations are drawn in red and egress scans in blue. (g) The SPICAM proton (white) and the SPICAM discrete aurora observations (black) are displayed on a map that shows the statistical Martian magnetic field intensity at 400 km altitude (taken from Connerney et al., 2001). (h) The histogram shows the distribution of all SPICAM limb observations selected for this study with respect to the solar cycle and Martian season (solar longitude L_S). The solid line represents the smoothed monthly sunspot number, and the red arrows indicate the six auroral observation dates (source of sunspot data: WDC-SILSO, Royal Observatory of Belgium, Brussels).

Table 1
Characteristics of the Proton Aurorae Observations

Orbit/ Sequence	Date	L_S (deg)	Scan	Time (hh:mm)	TP latitude (deg)	TP longitude (deg)	TP SZA (deg)	S/C altitude (km)	Bins	I_{aur} (kR)	TP altitude (km)	R_{int}	Solar trigger (observation comment)
1357/2	6/2/2005	156	I	17:16	55.4	198.8	49.3	333.7	N + W	0.7 ± 0.2	140.7	1.25	CME: possible; CIR: yes (Earth-Mars in near quadrature)
			E	17:25	22.8	202.8	30.8	679.3	N + W	1.2 ± 0.4	124.3	1.19	
1414/2	*22/2/2005*	*164*	*E*	*16:28*	*52.1*	*258.9*	*48.2*	*345.9*	*N + W*	–	*128.4*	*0.89*	*No aurora, reference case* Figure 1
1426/1	26/2/2005	166	I	01:02	71.7	300.9	74.5	351.2	N + W	1.1 ± 0.3	120.5	1.31	CME: possible; CIR: yes (Earth-Mars in near quadrature)
			E	01:08	53.8	260.6	50.3	347.6	N + W	3.0 ± 0.3	128.4	1.40	
2231/2	9/10/2005	303	E	10:33	−1.7	120.1	23.0	536.2	W	0.9 ± 0.2	148.3	1.02	CME: not likely; CIR: yes (Earth-Mars almost aligned)
2329/2	5/11/2005	319	I	20:40	−58.3	199.1	55.0	313.5	W	0.9 ± 0.2	140.6	1.17	CME: not likely; CIR: yes (Earth-Mars almost aligned)
			E	20:48	−30.1	216.0	30.2	328.9	W	1.5 ± 0.3	140.1	1.19	
4354/1	26/5/2007	245	I	20:44	−25.3	345.5	48.8	674.6	W	1.4 ± 0.2	140.5	1.15	CME: yes; CIR: no (Earth-Mars in quadrature)
4419/1	14/6/2007	257	E	01:19	−59.6	85.4	46.6	314.5	W	1.8 ± 0.5	132.4	0.98	CME: yes; CIR: no (Earth-Mars in quadrature)

Note. MEX *orbit number* and *observation sequence* are given, the date of the measurement and the corresponding Martian season (*solar longitude* L_S). The altitude scan is indicated by *I* (ingress) and *E* (egress). The *time* is given for the moment when the maximum intensity of the auroral feature is recorded. All following parameters refer to this moment. *Latitude*, *longitude*, and *solar zenith angle* (*SZA*) are listed for the tangent point (TP) as well as the *spacecraft altitude*. *N* and *W* indicate if the observation was recorded in the narrow, wide, or both bins. The auroral excess intensity I_{aur}, its uncertainty, and the *TP altitude* of the observation are given, followed by the intensity ratio R_{int}. The last column comments on the *solar trigger* and the observational condition for this trigger in parentheses. The table also includes italicized the parameters for Orbit 1414/2, which serves as reference orbit to Orbit 1426/1 in Figure 1. The italicized entries indicate the nonauroral case.

CMEs to Mars from 2007 onward. We could thus estimate if a CME should have reached Mars, or not, at the moment of the aurora. Furthermore, if Mars and the Earth were aligned, we used in situ data from ACE (located at the Sun-Earth L1 point) in order to verify a CME passage at Earth. If Mars and Earth are in quadrature, CMEs are seen starting from the west limb of the Sun toward Mars (note that for the events analyzed here Mars was always ahead of the Earth in its orbit, between approximately 0° and 180°).

For CIRs, we looked for coronal holes (in images of the Sun taken by SOHO Extreme ultraviolet Imaging Telescope and GOES Solar X-ray Imager), which were in position to create a fast solar wind stream that would arrive to Mars at the time of the aurora (around 60° west of the Sun-Mars line at the moment of the aurora and close to the solar equator). Since CIRs rotate with the Sun, we could use in situ data at the Earth orbit in order to identify them there and then calculate the time needed to reach Mars. If Earth and Mars are aligned, it is straightforward to predict the arrival of the CIR to Mars, applying a time delay based on Earth observations. If Earth and Mars are in quadrature, it takes about 8 days from the observations of the CIR at Earth until the plasma arrives at Mars (this time is calculated for each case, using the solar wind speed measured at the Earth).

4. Results

The SPICAM observations cover a time period from July 2004 to May 2011. From the observations with $R_{int} \geq 1.1$ we excluded three cases, as the enhancement was not found to be significant within the uncertainties. Two additional cases (MEX Orbit 2231/2 and MEX Orbit 4419/1) were identified with $R_{int} \leq 1.1$ but showing the auroral feature. In total, we found proton aurora signatures in 6 orbits out of 143: in 4 ingress and 5 egress cases, resulting in 9 limb profiles. For all six orbits we found CIRs and/or CMEs reaching Mars at the expected time.

Table 1 shows the study results, indicating several observational and spacecraft parameters for the time of the observations at which the maximum emission, denoted by I_{aur}, was recorded. The table includes also the identified solar trigger. Depending on the observational conditions, we judge the arrival of CME or CIR at Mars by "yes," "likely," "possible," "not likely," and "no."

Additionally, we found 12 cases during the visual inspection of the database, which show a marginal

enhancement at the considered altitudes. Most of these have $1.0 < R_{int} < 1.1$. Taking them into account, proton aurora could be found in as much as 13% of the orbits considered in this study. For most of these marginal auroral cases we do not have a clear identification of a possible solar trigger.

Figure 2 summarizes the results. Figures 2a–2f show the individual limb profiles of the identified aurorae that are listed in Table 1. Ingress scans are indicated in red and egress scans in blue. The altitude binning is 4 km, and the horizontal bars indicate the uncertainty on the mean value in each bin. The ingress scan of Orbit 2231/2 shows a marginal auroral case that we do not consider an auroral observation, and the egress scan of Orbit 4354/1 does not show an auroral signature. No ingress scan was obtained during Orbit 4419/1. Figure 2g displays the location of the observations on a statistical Martian crustal magnetic field intensity map (white stars). For comparison, we also show the locations of the discrete aurora observed by SPICAM, which is associated to magnetic field structures (black stars, from Gérard et al., 2015; Soret et al., 2016). Placing the observations utilized for this study in the context of the solar cycle (Figure 2h) shows that the SPICAM observations were obtained during the declining phase of solar cycle 24, during the unusual deep minimum in 2009, and in the rising phase of the following low solar maximum. Aurorae (red arrows) were only seen in the declining and minimum phase.

The comparison of all data from 2007 onward with the HELCATS ARRCAT catalogue revealed that for the SPICAM observations without aurora, no CME was predicted to reach Mars. Unfortunately, such a catalogue does not exist at the moment for CIRs.

5. Discussion

We observe proton aurora in 6 orbits out of 143, that is, in 4% of the observations. Their Lyman-α limb profiles show the auroral intensity peaks due to solar wind proton/hydrogen precipitation between 120 and 150 km. The half widths of the peak range from 110 up to 170 km in altitude and from 12 to almost 50 km in width. Assuming that the proton aurora is spatially homogeneous, the tangent point altitude shown in the figures is likely to be close to the true peak of the emission within the Martian atmosphere.

The observed excess brightness I_{aur} caused by the H^+-H precipitation is between 0.7 and 3.0 kR. The spacecraft altitude was between 300 and 700 km during the time of the measurements meaning the spacecraft observed the aurora always from above. Aurorae have been observed in the northern hemisphere and in the southern hemisphere of Mars and in regions with and without Martian crustal magnetic fields. A decrease in I_{aur} could be expected at locations of the magnetic field in response to the magnetic mirroring of a part of the precipitating protons (Diéval et al., 2013; Shematovich et al., 2011). However, our data set is not able to confirm this prediction due to lacking in situ proton flux measurements and the limited number of detections.

The cases when the proton aurora was seen in both, ingress and egress observations (Orbits 1357/2, 1426/1, and 2329/2), the change in longitude, latitude, solar zenith angle (SZA), and time gives a lower limit on the spatial and temporal extent of the aurora for these events. The latitudinal separations between ingress and egress scans span 18° to 35°. The fact that we observe differences in the auroral intensity for ingress and egress scans does not violate the approximation of a horizontally homogeneous emission. The latitudinal distances are large compared to the scale heights characterizing the integrated auroral Lyman-α emission along the LOS.

Orbit 2231/2 shows the weakest case of this study. We still consider it an aurora in egress, despite the low signal. The profile clearly deviates in the expected way from the commonly observed Lyman-α limb airglow profile, and a CIR was identified as solar trigger. The ingress scan we judge as a marginal increase (hence, it is neither listed in Table 1 nor shown on the magnetic field map in Figure 2). Comparing the observational parameters to the previously discussed orbits, they show no large differences in the spatial coverage or in the spacecraft altitude. This can either mean spatial restriction of the aurora or simply that the time of the auroral onset falls between ingress and egress scan or that the auroral emission was too weak to be detected unambiguously.

Orbit 4354/1 does not show an increase in the Lyman-α limb profile in egress, only in ingress. Noticeable is that the observation parameters change more than for the previously discussed orbits. The spacecraft altitude is about 1,000 km higher for the egress than for the ingress scan. The solar zenith angle equal to

78.8° is significantly larger for egress than for ingress (48.8°), but the change in location is similar to the other four cases.

In general, no dependence on the SZA of the tangent point is seen, even though one would expect a higher intensity at low SZA (Kallio & Barabash, 2001). However, the number of observations is limited and even though we identified the sources of the solar wind protons causing the aurora, their density and energy profile at Mars is unknown to us.

Halekas (2017, and references therein) reports a change in the column density of the hydrogen corona of Mars by an order of magnitude within one Martian year, peaking around southern summer solstice (L_S = 270°) close to perihelion. Unfortunately, due to the very limited data set, we are not able to confirm an effect neither on the proton aurora occurrence nor on its intensity.

It also should be noted that the proton aurora is not a discrete event. The increase in the solar wind density at the location of Mars can vary considerably depending on the strength of the solar event and its interplanetary transport (e.g., the solar wind density in different CMEs can vary by more than 1 order of magnitude). It also depends on the geometry of the encounter between the CME/CIR and Mars, as the density in the nose of a CME can be very different from that at its flank. The relatively large number of marginal cases found in this study and the example of Orbit 2231/2 indicate this smooth transition from a nonauroral case to a confirmed proton aurora.

Assessing the limb profiles in an automatic manner in order to find auroral features is not straightforward, as the resonant Lyman-α dayglow is quite variable and the excess emission not necessarily strongly pronounced. The selection criteria we used ($R_{\mathrm{int}} = I_{[120:150]\mathrm{km}}/I_{[160:190]\mathrm{km}}$) combined with visual inspection, however, proved to be reasonable for this survey. Other approaches included analysis of the distribution function of the intensities but did not lead to convincing results. Naturally, R_{int} depends on the altitude windows chosen, which is why the proton aurorae with a high and widespread altitude peak have not been correctly identified by this criteria: Orbit 2231/2 (R_{int} = 1.02) and Orbit 4419/1 (R_{int} = 0.98). It is likely that the altitude and the width of the peak depend on atmospheric density and temperature, as well as on the energy of the precipitating protons. This will be investigated with future modeling work.

6. Conclusion

Lyman-α emission signatures of proton aurora have been observed with the SPICAM ultraviolet spectrometer on board Mars Express between July 2004 and May 2011. Strong signatures have been found in 4% of the observations (6 out of 143 orbits) and weaker features in 12 additional cases. We do not claim presence of a proton aurora for the weak cases, but we neither exclude its presence. For all six strong cases we have found either a CME (two cases) and/or a CIR (four cases) reaching Mars at the time of the observations, which we believe triggered the auroral emission. The auroral excess intensity was up to 3 kR and peaks between 120 and 150 km. All confirmed observations have been made during the declining phase of solar cycle 24, which preceded the unusual deep solar minimum in 2009. This could be interpreted as an observational bias, but as the occurrence of CIRs is higher during the declining phase (Mursula & Zieger, 1996), we believe that this is a true effect. Observational parameters, like the spacecraft altitude or the solar zenith angle, might play a role for the detectability and the observed intensities, but we cannot present any correlation from the restricted data set at hand. For the same reason we cannot confirm the expected correlation with Martian season. Ongoing missions like MAVEN and future missions like the Trace Gas Orbiter are expected to provide a more complete data set of proton aurora observations, possibly including in situ observations of precipitating protons and ENAs produced in the Martian atmosphere. Further modeling work is needed to calculate the characteristics of the Lyman-α line profile and the expected altitude and intensity distribution for conditions of enhanced solar wind activity.

Acknowledgments
The authors thank J. Deighan and the IUVS team and acknowledge their finding of the proton aurora. We also thank both reviewers for their highly constructive comments. Mars Express is an ESA mission. B. R. acknowledges support from the Brain/SCOOP research program of the Belgian Federal Science Policy Office (BELSPO). This research was partly funded by the NOMAD PRODEX program managed by the European Space Agency with help of BELSPO. L. R. acknowledges support from the Interuniversity Attraction Poles Program initiated by BELSPO (IAP P7/08 CHARM) and from the European Union FP7 Program (606692, HELCATS). The authors thank the SPICAM instrumental team for the SPICAM data and calibration and specifically G. Lacombe and L. Baggio for their support. The SPICAM/MEX data used in this study are available through the ESA Planetary Science Archive (PSA, https://archives.esac.esa.int/psa/). The SOHO LASCO CME catalogue is available at https://cdaw.gsfc.nasa.gov/CME_list, and the HELCATS ARRCAT catalogue is available at https://www.helcats-fp7.eu/catalogues/wp4_arrcat.html.

References

Barabash, S., Lundin, R., Zarnowiecki, R., & Grzedzielski, S. (1995). Diagnostic of energetic neutral particles at Mars by the ASPERA-C instrument for the Mars 96 mission. *Advances in Space Research*, *16*(4), 81–86. https://doi.org/10.1016/0273-1177(95)00212-W

Bertaux, J.-L., Korablev, O., Perrier, S., Quémerais, E., Montmessin, F., Leblanc, F., … Guibert, S. (2006). SPICAM on Mars Express: Observing modes and overview of the spectrometer data and scientific results. *Journal of Geophysical Research*, *111*, E10S90. https://doi.org/10.1029/2006JE002690

Bertaux, J.-L., Leblanc, F., Witasse, O., Quemerais, E., Lilensten, J., Stern, S. A., … Korablev, O. (2005). Discovery of an aurora on Mars. *Nature*, *435*(7043), 790–794. https://doi.org/10.1038/nature03603

Chaufray, J. Y., Bertaux, J.-L., Leblanc, F., & Quémerais, E. (2008). Observation of the hydrogen corona with SPICAM on Mars Express. *Icarus*, *195*(2), 598–613. https://doi.org/10.1016/j.icarus.2008.01.009

Connerney, J. E. P., Acuña, M. H., Wasilewski, P. J., Kletetschka, G., Ness, N. F., Rème, H., … Mitchell, D. L. (2001). The global magnetic field of Mars and implications for crustal evolution. *Geophysical Research Letters*, *28*(21), 4015–4018. https://doi.org/10.1029/2001GL013619

Diéval, C., Stenberg, G., Nilsson, H., Edberg, N. J. T., & Barabash, S. (2013). Reduced proton and alpha particle precipitations at Mars during solar wind pressure pulses: Mars Express results. *Journal of Geophysical Research: Space Physics*, *118*, 3421–3429. https://doi.org/10.1002/jgra.50375

Eather, R. H. (1967). Auroral proton precipitation and hydrogen emissions. *Reviews of Geophysics and Space Physics*, *5*(3), 207–285. https://doi.org/10.1029/RG005i003p00207

Futaana, Y., Barabash, S., Grigoriev, A., Holmström, M., Kallio, E., Brandt, P. C., … Dierker, C. (2006). First ENA observations at Mars: ENA emissions from the Martian upper atmosphere. *Icarus*, *182*(2), 424–430. https://doi.org/10.1016/j.icarus.2005.09.019

Gérard, J.-C., Hubert, B., Meurant, M., Shematovich, V. I., Bisikalo, D. V., Frey, H., … Carlson, C. W. (2001). Observation of the proton aurora with IMAGE FUV imager and simultaneous ion flux in situ measurements. *Journal of Geophysical Research*, *106*(A12), 28,939–28,948. https://doi.org/10.1029/2001JA900119

Gérard, J.-C., Soret, L., Libert, L., Lundin, R., Stiepen, A., Radioti, A., & Bertaux, J.-L. (2015). Concurrent observations of ultraviolet aurora and energetic electron precipitation with Mars Express. *Journal of Geophysical Research: Space Physics*, *120*, 6749–6765. https://doi.org/10.1002/2015JA021150

Halekas (2017). Seasonal variability of the hydrogen exosphere of Mars. *Journal of Geophysical Research: Planets*, *122*, 901–911. https://doi.org/10.1002/2017JE005306

Halekas, J. S., Lillis, R. J., Mitchell, D. L., Cravens, T. E., Mazelle, C., Connerney, J. E. P., … Ruhunusiri, S. (2015). MAVEN observations of solar wind hydrogen deposition in the atmosphere of Mars. *Geophysical Research Letters*, *42*, 8901–8909. https://doi.org/10.1002/2015GL064693

Halekas, J. S., Ruhunusiri, S., Harada, Y., Collinson, G., Mitchell, D. L., Mazelle, C., … Jakosky, B. M. (2017). Structure, dynamics, and seasonal variability of the Mars-solar wind interaction: MAVEN solar wind ion analyzer in-flight performance and science results. *Journal of Geophysical Research: Space Physics*, *122*, 547–578. https://doi.org/10.1002/2016JA023167

Hubert, B., Gérard, J.-C., Bisikalo, D. V., Shematovich, V. I., & Solomon, S. C. (2001). The role of proton precipitation in the excitation of auroral FUV emissions. *Journal of Geophysical Research*, *106*(A10), 21,475–21,494. https://doi.org/10.1029/2000JA000288

Jian, L., Russell, C. T., Luhmann, J. G., & Skoug, R. M. (2006). Properties of stream interactions at one AU during 1995–2004. *Solar Physics*, *239*(1-2), 337–392. https://doi.org/10.1007/s11207-006-0132-3

Kallio, E., & Barabash, S. (2001). Atmospheric effects of precipitating energetic hydrogen atoms on the Martian atmosphere. *Journal of Geophysical Research*, *106*(A1), 165–177. https://doi.org/10.1029/2000JA002003

Kallio, E., Luhmann, J. G., & Barabash, S. (1997). Charge exchange near Mars: The solar wind absorption and energetic neutral atom production. *Journal of Geophysical Research*, *102*(A10), 22,183–22,197. https://doi.org/10.1029/97JA01662

Kilpua, E. K. J., Lumme, E., Andreeova, K., Isavnin, A., & Koskine, H. E. J. (2015). Properties and drivers of fast interplanetary shocks near the orbit of the Earth (1995–2013). *Journal of Geophysical Research: Solar Physics*, *120*, 4112–4125. https://doi.org/10.1002/2015JA021138

Leblanc, F., Chaufray, J. Y., Witasse, O., Lilensten, J., & Bertaux, J.-L. (2006). The Martian dayglow as seen by SPICAM UV spectrometer on Mars Express. *Journal of Geophysical Research*, *111*, E09S11. https://doi.org/10.1029/2005JE002664

Leblanc, F., Luhmann, J. G., Johnson, R. E., & Chassefière, E. (2002). Some expected impacts of a solar energetic particle event at Mars. *Journal of Geophysical Research*, *107*(A5), 1058. https://doi.org/10.1029/2001JA900178

Lundin, R., Barabash, S., Andersson, H., Holmström, M., Grigoriev, A., Yamauchi, M., … Bochsler, P. (2004). Solar wind-induced atmospheric erosion at Mars: First results from ASPERA-3 on Mars Express. *Science*, *305*(5692), 1933–1936. https://doi.org/10.1126/science.1101860

Montmessin, F., Korablev, O., Lefèvre, F., Bertaux, J.-L., Fedorova, A., Trokhimovskiy, A., … Chapron, N. (2017). SPICAM on Mars Express: A 10 year in-depth survey of the Martian atmosphere. *Icarus*, *297*, 195–216. https://doi.org/10.1016/j.icarus.2017.06.022

Möstl, C., Isavnin, A., Boakes, P. D., Kilpua, E. K. J., Davies, J. A., Harrison, R. A., … Zhang, T. L. (2017). Modeling observations of solar coronal mass ejections with heliospheric imagers verified with the Heliophysics System Observatory. *Space Weather*, *15*, 955–970. https://doi.org/10.1002/2017SW001614

Mursula, K., & Zieger, B. (1996). The 13.5-day periodicity in the Sun, solar wind, and geomagnetic activity: The last three solar cycles. *Journal of Geophysical Research*, *101*(A12), 27,077–27,090. https://doi.org/10.1029/96JA02470

Rodriguez, L., Masías-Meza, J. J., Dasso, S., Démoulin, P., Zhukov, A. N., Gulisano, A. M., … Janvier, M. (2016). Typical profiles and distributions of plasma and magnetic field parameters in magnetic clouds at 1 AU. *Solar Physics*, *291*(7), 2145–2163. https://doi.org/10.1007/s11207-016-0955-5

Schneider, N. M., Deighan, J. I., Jain, S. K., Stiepen, A., Stewart, A. I. F., Larson, D., … Jakosky, B. M. (2015). Discovery of diffuse aurora on Mars. *Science*, *350*(6261). https://doi.org/10.1126/science.aad0313

Shematovich, V. I., Bisikalo, D. V., Diéval, C., Barabash, S., Stenberg, G., Nilsson, H., … Gérard, J.-C. (2011). Proton and hydrogen atom transport in the Martian upper atmosphere with an induced magnetic field. *Journal of Geophysical Research*, *116*, A11320. https://doi.org/10.1029/2011JA017007

Soret, L., Gérard, J.-C., Libert, L., Shematovich, V. I., Bisikalo, D. V., Stiepen, A., & Bertaux, J.-L. (2016). SPICAM observations and modeling of Mars aurorae. *Icarus*, *264*, 398–406. https://doi.org/10.1016/j.icarus.2015.09.023

Vegard, L. (1939). Hydrogen showers in the auroral region. *Nature*, *144*, 1089.

Wang, X.-D., Barabash, S., Futaana, Y., Grigoriev, A., & Wurz, P. (2013). Directionality and variability of energetic neutral hydrogen fluxes observed by Mars Express. *Journal of Geophysical Research: Space Physics*, *118*, 7635–7642. https://doi.org/10.1002/2013JA018876

Webb, D. F., & Howard, T. A. (2012). Coronal mass ejections: Observations. *Living Reviews in Solar Physics*, *9*, 3. http://www.livingreviews.org/lrsp-2012-3